# Volume Parameterization for Design Automation of Customized Free-Form Products

Charlie C. L. Wang, *Member, IEEE*, K.-C. Hui, and K.-M. Tong

***Abstract*—This paper addresses the problem of volume parameterization that serves as the geometric kernel for design automation of customized free-form products. The purpose of volume parameterization is to establish a mapping between the spaces near to two reference free-form models, so that the shape of a product presented in free-form surfaces can be transferred from the space around one reference model to another reference models. The mapping is expected to keep the spatial relationship between the product model and reference models as much as possible. We separate the mapping into rigid body transformation and elastic warping. The rigid body transformation is determined by anchor points defined on the reference models using a least-square fitting approach. The elastic warping function is more difficult to obtained, especially when the meshes of the reference objects are inconsistent. A three-stage approach is conducted. Firstly, a coarse-level warping function is computed based on the anchor points. In the second phase, the topology consistency is maintained through a surface fitting process. Finally, the mapping of volume parameterization is established on the surface fitting result. Comparing to previous methods, the approach presented here is more efficient. Also, benefited from the separation of rigid body transformation and elastic warping, the transient shape of a transferred product does not give unexpected distortion. At the end of this paper, various industry applications of our approach in design automation are demonstrated.**

***Note to Practitioners*—The motivation of this research is to develop a geometric solution for the design automation of customized free-form objects, which can greatly improve the efficiency of design processes in various industries involving customized products (e.g., garment design, toy design, jewel design, shoe design, and glasses design, etc.). The products in the above industries are usually composed of very complex geometry shape (represented by free-form surfaces), and is not driven by a parameter table but a reference object with free-form shapes (e.g., mannequin, toy, wrist, foot, and head models). After carefully designing a product around one particular reference model, it is desirable to have an automated tool for "grading" this product to other shape-changed reference objects while retaining the original spatial relationship between the product and reference models. This is called the design automation of customized freeform object. Current commercial 3D/2D Computer-Aided Design (CAD) systems, developed for the design automation of models with regular shape, cannot support the design automation in this manner. The approach in this paper develops efficient techniques for constraining and reconstructing a product represented by freeform surfaces around reference objects with different shapes, so that this design automation problem can be fundamentally solved. Although the approach has not been integrated into commercial CAD systems, the results based on our preliminary implementation are encouraging – the spatial relationship between reference models and the customized products is well preserved.**

***Index Terms*—Deformation, design automation, free-form objects, radial-basis function.**

The authors are with the Department of Automation and Computer-Aided Engineering, Chinese University of Hong Kong, Shatin, N.T., Hong Kong (phone: 852-26098052; fax: 852-26036002; e-mail: cwang@acae.cuhk.edu.hk or wangcl@ieee.org).

## I. Introduction

THE design automation functions provided in current commercial CAD/CAM/CAE systems are developed for products with regular shapes. This kind of design automation is usually driven by dimensional parameters, so called parametric design [1-3]. However, the products in industries like apparel, toy, jewel, shoe, and glasses etc. are usually composed of complex geometry represented by freeform surfaces, and with their shape adjusted by the reference models "wearing" the products. In these industries, after carefully designing a product around one particular reference model, it is desirable to have an automatic process that can "grade" this product to other reference objects with shapes varied while maintaining the spatial relationship on the original design. This is called the *design automation* of customized freeform object. The purpose of this research is to develop a fundamental technique – volume parameterization for supporting this design automation.

Consider two reference objects $H_a$ and $H_b$, which are represented by free-form polygonal meshes, a volume parameterization as referred to here is a forward mapping $\Psi:\Omega_a \to \Omega_b$ from any point $p$ in the space $\Omega_a \subset \Re^3$ around $H_a$ to a corresponding point $p'$ in the space $\Omega_b \subset \Re^3$ around $H_b$. Based on $\Psi$, a product $\mathrm{M}$ originally designed around $H_a$, which is also represented by free-form polygonal meshes, could be transferred to the shape around $H_b$ by mapping the position of every vertex on $\mathrm{M}$ into a new position in $\Omega_b$. In the design automation applications, the mapping $\Psi$ is expected to be sensitive to semantic features on the reference models, which is usually described by anchor points. Therefore, two set of anchor points, $G_a$ and $G_b$, are assigned on $H_a$ and $H_b$ – the anchor points are one-to-one mapped which could be either automatically extracted or interactively specified. The correspondences of the anchor points give the relationship of

semantic features on the reference models. Particularly, more anchor points are given, more accurate mapping $\Psi$ could be computed. The mapping $\Psi$ is also expected to provide a smooth transition between $\Omega_a$ and $\Omega_b$ (i.e., the mapping $\Psi(t)$ is a smooth function with the transient variable $t \in [0,1]$). The mesh connectivity on $H_a$ and $H_b$ are generally inconsistent. The previous approaches presented in [4-7], which all require consistent connectivity, cannot be directly applied to establish the mapping $\Psi$. Although the meshes on reference models are not necessarily the same, they usually have similar features. In other words, there is little use of transferring the clothes on a human body to a cup. Our volume parameterization technique makes use of this characteristic to compute $\Psi$ on the reference models with different meshes.

In order to provide a smooth transition property in $\Psi$, we separate the mapping into two sub-mappings: 1) rigid body transformation and 2) elastic warping. The rigid body transformation is usually represented by a rotation matrix $R(\theta_x, \theta_y, \theta_z)$ and a translation vector $T$. We determine $R(\theta_x, \theta_y, \theta_z)$ and $T$ through a least-square fitting process. The procedure of computing the elastic warping component in the mapping $\Psi$ is more complex. A three-stage approach is developed for this, which starts from computing a coarse-level warping function by anchor points. After applying the coarse-level warping function on the mesh surface of $H_a$, we obtain a warped $H_a'$. The shapes of $H_a'$ and $H_b$ are similar to each other such that a surface fitting process can be applied on $H_a'$ to match its connectivity to that of $H_b$. A bijective correspondence is therefore established between the surfaces of $H_a$ and $H_b$ (this correspondence is also called *cross-surface parameterization* [8, 9]). By the cross-surface parameterization, we could finally construct the mapping $\Psi$ in two manners, either using *Compactly Supported Radial-Basis Function* – CSRBF or using polygon driven *Free-Form Deformation* – p-FFD [7].

As will be discussed in detail, the contribution of our volume parameterization framework includes:

1) The volume parameterization technique proposed in this paper provides a geometric framework for the design automation of customized free-form products;
2) The mapping of spaces around reference models is established without the restriction of having the same connectivity on the reference models;
3) The mapping of parameterization could be constructed both mathematically and algorithmically, where the CSRBF description can be repeatedly used for the design automation of other products on the same two references models, while the p-FFD result needs to be recomputed every time when a new product is considered – thus the CSRBF-based method presented in this paper is more efficient;
4) Based on the separation of rigid body transformation and elastic warping, the mapping $\Psi$ provides a smooth transformation between $\Omega_a$ and $\Omega_b$, which is important for the serials "grading" – so that unwanted distortions are avoided on the transient results;
5) The mapping method described in this paper is compact and easy to implement since the mapping is mathematically defined instead of complex algorithmic procedures.

In more detail, comparing the technique presented in this paper with our previous work [7], novelties are shown in three aspects:

- The constraint about the consistent mesh connectivity on reference models is overcome, i.e., as long as the reference models are with the similar features, the mapping $\Psi$ between them can be established.
- Based on the mathematical mapping function which separate the rigid transformation and the elastic deformation, a smooth transition can be achieved on $\Psi(t)$ with the transient variable $t \in [0,1]$.
- Lastly also the most important one is that, the mapping defined mathematically by CSRBF is more compact and efficient since the same mapping is employed when new products are introduced – the mapping needs not to be recomputed.

The rest of this paper is organized as follows. After reviewing related techniques, the methodology of constructing a volume parameterization is introduced in section III. The details of numerical implementation are then presented in the following section. Finally, through experimental results and applications, we show that the proposed method successfully transfers products with free-form surface from one reference model to another model while maintaining the spatial relationship in between.

## II. Related work

In this section, we successively review related techniques about surface and cross-surface parameterization, free-form deformation, and radial-basis functions (RBFs).

### A. Surface and Cross-Surface Parameterization

The parameterization of mesh surface is actually a process of flattening 3D meshes, which provides a bijective mapping between the mesh and a planar polygon. If two meshes are mapped into the same planar polygon, the bijective mapping could also be constructed between 3D meshes. An excellent survey of recent advances in mesh parameterization is given in [10], see also the references therein. Floater [11] investigated a graph-theory based parameterization on tessellated surfaces for the purpose of smooth surface fitting; his parameterization (actually a planar triangulation) is the solution of linear systems based on convex combination. Most recent approaches [12-19] of surface parameterization focused on how to construct a conformal mapping between the 3D mesh and the planar polygon, while trying to minimize the length distortion (i.e., isometric mapping is desired).

The above planar parameterization approaches have the

limitation that a closed surface needs to be cut into one or more disk-like charts, where each chart is then parameterized independently. As mentioned in [9], the cuts break the continuity of the parameterization, and make it difficult to construct a continuous map between two *different* mesh surfaces. Thus, the cross-surface parameterization without cutting is required. The cross-surface parameterization is typically computed by registering the model onto a common based domain (ref. [20-25], where Alexa [20] gives a detail review of cross-parameterization and compatible remeshing techniques for three-dimensional morphing). Recently, in [8], the authors computed a low-distortion bijective mapping between models while satisfying user predefined feature constraints – also in the form of anchor points. The approach in [9] addressed the same problem but using progressive mesh as intermedium.

Allen et al. [26] used the connectivity of one mesh to approximate the connectivity of another, avoiding explicit parameterization. Since in design automation, the reference models usually have similar shapes, we construct the mapping between reference models by a method akin to [26] but with faster computation time. So far, all surface parameterization or cross-surface parameterization approaches considered only points on the given surfaces. In this paper, we address the problem of mapping points in the spaces around given mesh models, in which there is not much published work found in the literature.

In the area of industrial design, there are some works related to our research in the name of parametric design of free-form models (e.g., [27, 28]), where the work in [27] conducted a feature-template matching method to recognize freeform features and their parameters, and [28] worked on the dimension driven parameterized design of free-form objects where the purpose is to obtain a new free-form object similar in shape to the old one but with different set of dimension instantiations.

### B. Free-Form Deformation and Warping

Free-Form Deformation (FFD) [29] and its variants [30-33] take an important role in geometric modeling, where a free-form object to be deformed are embedded inside a volume which is usually parametrically represented. When the volume is deformed, the embedded free-form objects are transformed to a new shape by keeping the parameters relative to the volume at every vertex. FFDs are useful for coarse-scale deformations but not finer-scale deformations even if a very dense lattice or customized lattice shape is defined. The t-FFD approach [6] adopts triangles as deformation primitives so that detail deformation control could be achieved. However, as mentioned before, t-FFD cannot be directly applied to construct the mapping $\Psi$ for volume parameterization since the consistent connectivity on reference models is required. The last step in our algorithm-based solution of volume parameterization could also adopt a similar approach – p-FFD [7] to finish the elastic warping, where polygonal facets of reference models are utilized as deformation drivers.

In [34], Hua and Qin proposed a scalar-field-guided adaptive shape deformation technique, where a displacement or velocity field is generated upon the deformation of a scalar field resulting in a shape deformation of the embedded objects. Their approach actually provided an implicit solution for the volume parameterization. If two distance-field $D_a$ and $D_b$ are computed around $H_a$ and $H_b$ correspondingly, when a velocity field is constructed on the deformation from $D_a$ and $D_b$, one solution of volume parameterization is given by embedding the free-form product $\mathrm{M}$ of $H_a$ in the velocity field. However, three problems arise: 1) this is an implicit solution (i.e., the mapping $\Psi$ is not explicitly given), which leads to a long computing time; 2) every time when a new product is considered, the mapping between $H_a$ and $H_b$ needs to be recomputed – this is definitely inefficient; 3) the deformation is not sensitive to rotations on the reference models. For the third problem, the authors in [35] separate the deformation into a rigid body transformation $\Gamma$ and an elastic warping $\mathrm{E}$ so that smooth transient results could be achieved. In this work, we applied a similar separation. However, it is found that the order of applying $\Gamma$ and $\mathrm{E}$ in [33] may affect the smoothness in transient results. Thus, an alternative method is developed.

Some others [36, 37] did the research similar to ours in the framework of animation. In their approaches, the affine transformation is separated from the deformation instead of the rigid one. In our approach, since the affine transformation terms have been included in the RBF and CSRBF, we only separate the rigid transformation out.

### C. Radial-Basis Functions

Nowadays, radial-basis functions (RBFs) have been widely employed in various areas of geometric modeling – for example, RBFs based surface reconstruction [38-42], RBFs based metamorphosis [35, 43], RBFs based geometry and image processing [44], and RBFs based semantic parametric design [5, 45, 46]. The RBFs could be classified into the ones having global effect and the compactly supported RBFs (CSRBFs) with local effect. The procedure of determining coefficients in RBFs involves the step of solving a linear equation system. The sparseness of CSRBFs makes it possible to have a fast solution when the number of interpolates is huge. Therefore, in our approach, the preliminary warping function at the coarse-level adopts global RBFs interpolating anchor points whose number is usually few, and CSRBFs are conducted to define the final warping function in $\Psi$ with thousands of interpolates involved.

## III. Methodology

This section describes the methodology of volume parameterization. To construct a mapping $\Psi$ satisfying the requirements listed above, we successively address the issues about how to separate the rigid body transformation and the elastic warping, how to find the cross-surface correspondences, and how to finally establish the integrated mapping with

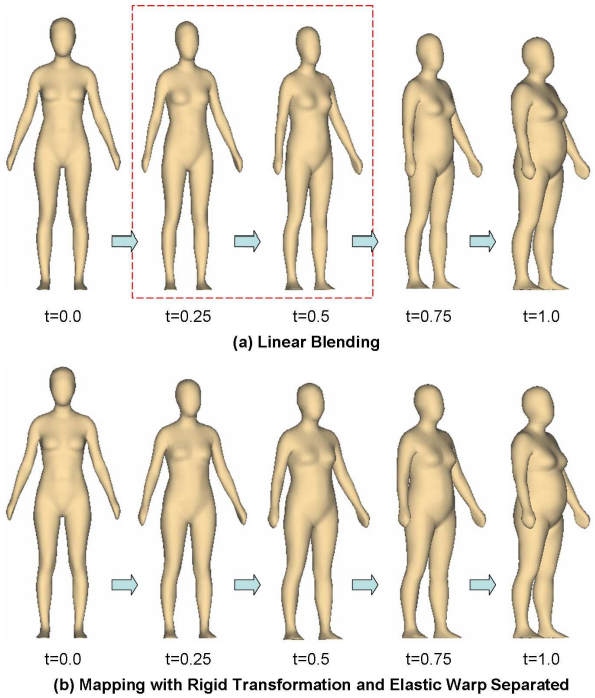


Fig. 1. The transient results of linear blending (top row) have unwanted distortion – the model becomes very thin and narrow (the 2nd and the 3rd model at the top row), i.e., the model between the first and the last models is even thinner than themselves, which is not reasonable; the results from the mapping with rigid body transformation and elastic warping (bottom row) are smooth.

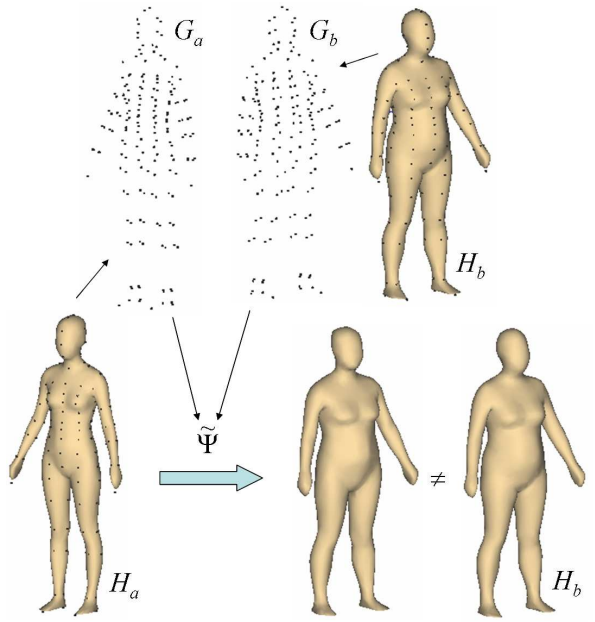


Fig. 2. After applying the transformation and warping (generated by anchor points) on the surface of reference model $H_a$, the result surface is still somewhat different from the surface of $H_b$.

transformation and warping.

### A. Rigid Body Transformation and Anchors Based Warping

Without loss of general, let us assume that the correspondences have been constructed between points in the spaces $\Omega_a$ and $\Omega_b$ of two reference models $H_a$ and $H_b$. The simplest transient mapping $\Psi(t)$ between $\Omega_a$ and $\Omega_b$ is a linear blending: $\Psi(t) = (1-t)\Omega_a + t\Omega_b$ with $t \in [0,1]$. However, as demonstrated in Fig. 1, linear blending is not sensitive to the orientation of the reference objects where unexpected distortion may be obtained. Thus, we partition the mapping between $\Omega_a$ and $\Omega_b$ into a rigid body transformation $\Gamma(q) \equiv R(\theta_x, \theta_y, \theta_z)q + T$ and an elastic warping $\mathrm{E}(\cdots)$ with $\Gamma(\mathrm{E}(\Omega_a)) \equiv \Omega_b$ and hence,

$$\Psi(t) = R(t\theta_x, t\theta_y, t\theta_z)((1-t)\Omega_a + t\mathrm{E}(\Omega_a)) + tT \,. \quad (1)$$

The rotation matrix $R(\theta_x, \theta_y, \theta_z)$ and the translation vector $T$ can be determined in a least-square sense by minimizing the following energy function defined on the anchor points ($G_a$ and $G_b$ prescribed on the reference models)

$$J = \sum_{q \in G_a} \left\| R(\theta_x, \theta_y, \theta_z)q + T - q' \right\|^2 , \quad (2)$$

where $q' \in G_b$ is the corresponding anchor point of $q \in G_a$ and $\|\cdots\|$ is the Euclidean norm on $\Re^3$.

After determining the rigid body transformation $\Gamma(\cdots)$, the elastic warping $\mathrm{E}(\cdots)$ also needs to be computed. A coarse-level warping function is expected to be a nonlinear transformation $\tilde{\mathrm{E}}: \Re^3 \to \Re^3$ such that

$$\tilde{\mathrm{E}}(q) = \Gamma^{-1}(q') \quad (q \in G_a \text{ and } q' \in G_b) \quad (3)$$

with $\Gamma^{-1}(q') \equiv R(-\theta_x, -\theta_y, -\theta_z)(q' - T)$. Since the anchor points in $G_b$ have been transformed backwards by $\Gamma^{-1}(q')$ to have the same center and orientation with the points in $G_a$, the elastic function determined by Eq.(3) will not be affected by the change in orientations of the reference models. The hybrid of $\Gamma(\cdots)$ and $\tilde{\mathrm{E}}(\cdots)$ is expected to map corresponding anchor points exactly. This is in fact a multivariable scattered data interpolation problem, which we propose to solve by using radial basis functions. The determined mapping based on anchor points is denoted by $\tilde{\Psi}$. The implementation details will be presented in the A and B parts of section IV.

### B. Cross-surface Correspondences

The elastic warping function determined by interpolating anchor points only accurately controls the warping near anchor points. For the space between anchor points, the warping is not well defined. For example in Fig. 2, after applying the transformation and warping (generated by anchor points) on the surface of $H_a$, the surface obtained is still somewhat different from the surface of $H_b$. In order to have a more accurate mapping, we need to increase the number of corresponding points on the surfaces of $H_a$ and $H_b$. This is achieved through a procedure of surface fitting.

Surface fitting is performed by minimizing an energy function defined by the differences between the surfaces of $\tilde{\mathrm{E}}(H_a)$ and $H_b'$ (with $H_b' = \Gamma^{-1}(H_b)$) and the smoothness term on the resultant surface. In fact, the surface fitting process is an evolution of $\tilde{\mathrm{E}}(H_a)$ to obtain a deformed model $H_a'$, which has its shape approximates $H_b'$ and maintains the same mesh connectivity on $H_a$. The numerical scheme for this step is detailed in the part C of section IV.

### C. Volume Parameterization

With the help of $H_a'$, a finer-level correspondences between points on the surfaces of $H_a$ and $H_b'$ is obtained. Therefore, an accurate mapping $\Psi(t)$ defined in Eq.(1) for volume parameterization can be established by computing an accurate elastic function $\mathrm{E}(\cdots)$ based on the position of vertices on $H_a$ and $H_a'$. The elastic function $\mathrm{E}(\cdots)$ is then evaluated in the manners of CSRBF. To compare with our previous work, p-FFD is also conducted to define $\mathrm{E}(\cdots)$ implicitly.

For the CSRBF-based solution, we determine the coefficients of compactly supported radial-basis functions (CSRBFs) by solving the linear equation system describing the position correspondences of vertices on $H_a$ and $H_a'$. The compact supporting property of CSRBFs makes the linear equation system very sparse, so that it can be solved efficiently. Details see the part D in section IV.

$\mathrm{E}(\cdots)$ could also be defined (but implicitly) using p-FFD. Every vertex on $\mathrm{M}$ around $H_a$ is first encoded by its coordinates relative to the local coordinate frames on its *k*-nearest polygons on $H_a$. These coordinates are stored and used for mapping to a new position when the shape on $H_a'$ is applied instead of $H_a$. The distances from a vertex to the centers of the corresponding polygons serve as weights. This is called p-FFD since the geometry of $\mathrm{M}$ is deformed in the FFD sense but with polygons on $H_a$ and $H_a'$ as deformation primaries. The implementation detail (see the part E of section IV) is more or less similar to our previous work [7].

## IV. Numerical Implementation

The numerical implementation details of our volume parameterization approach are presented in this section.

### A. Rigid Body Transformation

We determine the rotation matrix $R(\theta_x, \theta_y, \theta_z)$ and the translation vector $T$ by the anchor points in $G_a$ and $G_b$. According to Arun et al. [47], if the solution of Eq.(1) is $\hat{R}$ and $\hat{T}$, $G_b$ and $\hat{R}G_a + T$ have the same centroid, Eq.(1) can be simplified by introducing a transfer of coordinate:

$$p_i = q_i - c_a,\ (q_i \in G_a) \text{ and } p_i' = q_i' - c_b,\ (q_i' \in G_b) \qquad (4)$$

where $c_a$ and $c_b$ are the centroids of $G_a$ and $G_b$, and there are *N* anchor points. Thus, Eq.(2) can be rewritten as

$$J' = \sum_{i=1}^{N} \left\| \hat{R}p_i - p_i' \right\|^2 \qquad (5)$$

since $c_b \equiv \hat{R}c_a + \hat{T}$. As long as $N > 3$, let

$$\partial J' / \partial \hat{R} = 0 \qquad (6)$$

the $3\times3$ matrix $\hat{R}$ can be solved by the singular value decomposition method (SVD) [48], and the translation vector $T = \hat{T}$ is determined by $c_b \equiv \hat{R}c_a + \hat{T}$. Note that the $\hat{R}$ determined by Eq.(3) is a global minimum since the objective function $J'$ is in the quadratic form. The SVD determined $\hat{R}$ needs to be first converted into a quaternion $[w, (x, y, z)]$. The components of the quaternion are then normalized by setting $w^2 + x^2 + y^2 + z^2 = 1$. Finally, the Euler angles $\theta_x$, $\theta_y$, and $\theta_z$ can be separated from the normalized quaternion so that the rotation matrix $R(\theta_x, \theta_y, \theta_z)$ is finalized. Details of this conversion are stated in [49]. Once $R(\theta_x, \theta_y, \theta_z)$ and $T$ are determined, the rigid body transformation $\Gamma(\cdots)$ is defined.

### B. RBF-based Elastic Function

A coarse-level elastic function is defined as a function $\tilde{\mathrm{E}}(q)$ to map every anchor point $q \in G_a$ exactly onto the position $\Gamma^{-1}(q')$ with $q' \in G_b$ (see Eq.(3)). As mentioned above, this is a multivariable interpolation problem, where RBFs are the most efficient candidate to formulate $\tilde{\mathrm{E}}(q)$. Thus, an elastic warping function of the following form is considered

$$\tilde{\mathrm{E}}(q) = \alpha_0 + Aq + \sum_{i=0}^{N} \beta_i g(\left\| q - q_i \right\|). \qquad (7)$$

where $\alpha_0$ and $A$ controls the affine transformation of points, and the third term in $\tilde{\mathrm{E}}(q)$ defined the rest nonlinear warping. Here the $\left\| \cdot\cdot \right\|$ denotes the Euclidean norm on $\Re^3$, and $A = (\alpha_1, \alpha_2, \alpha_3)^T$. The coefficients $\beta_i \in \Re^3$ ($1 \le i \le n$) and $\alpha_l \in \Re^3$ ($0 \le l \le 3$) are unknowns to be determined by the following interpolation constraints:

$$\tilde{\mathrm{E}}(q_i) \equiv \Gamma^{-1}(q_i') = R(-\theta_x, -\theta_y, -\theta_z)(q_i' - T), \quad i = 1, \cdots, N, \qquad (8)$$

The form of $g(\cdots)$ needs to be determined first. As analyzed, in the coarse-level elastic function we expect to have a global effect, so that $g(r) = r^3$ following [35, 42, 50] is adopted. There are 3(*N*+4) unknowns but with only 3*N* conditions on the above interpolation requirements (i.e., Eq.(8)). To avoid this uncertainty, the following compatibility conditions are usually

added

$$\sum_{i=1}^{N}\beta_i^k=\sum_{i=1}^{N}\beta_i^k q_i^1=\sum_{i=1}^{N}\beta_i^k q_i^2=\sum_{i=1}^{N}\beta_i^k q_i^3=0,\quad k=1,2,3. \tag{9}$$

By adopting $g_{ij}$ to denote $g(\|q_i-q_j\|)$, the linear equation system to determine $\tilde{\mathrm{E}}(q)$ can be written as

$$\begin{bmatrix} g_{11} & g_{12} & \cdots & g_{1N} & 1 & q_1^1 & q_1^2 & q_1^3 \\ g_{21} & g_{22} & \cdots & g_{2N} & 1 & q_2^1 & q_2^2 & q_2^3 \\ \vdots & \vdots & \ddots & \vdots & \vdots & \vdots & \vdots & \vdots \\ g_{1N} & g_{2N} & \cdots & g_{NN} & 1 & q_N^1 & q_N^2 & q_N^3 \\ 1 & 1 & \cdots & 1 & 0 & 0 & 0 & 0 \\ q_1^1 & q_2^1 & \cdots & q_N^1 & 0 & 0 & 0 & 0 \\ q_1^2 & q_2^2 & \cdots & q_N^2 & 0 & 0 & 0 & 0 \\ q_1^3 & q_2^3 & \cdots & q_N^3 & 0 & 0 & 0 & 0 \end{bmatrix}\begin{bmatrix}\beta_1\\ \beta_2\\ \vdots\\ \beta_N\\ \alpha_0\\ \alpha_1\\ \alpha_2\\ \alpha_3\end{bmatrix}=\begin{bmatrix}\Gamma^{-1}(q_1')\\ \Gamma^{-1}(q_2')\\ \vdots\\ \Gamma^{-1}(q_N')\\ 0\\ 0\\ 0\\ 0\end{bmatrix}. \tag{10}$$

The system is symmetric and positive definite unless all $q_i$ s are coplanar, which seldom happens in practice. Based on this constraint, the number of anchor points should be more than 3 and they must not be coplanar. Therefore, there exists a unique solution of $\tilde{\mathrm{E}}(q)$ [51]. The number of anchor points usually is at the level of tens, so that Gaussian elimination [48] is adopted to solve Eq.(10) directly.

### C. Surface Fitting

To seek a fine-level correspondences of points on the surfaces of $H_a$ and $H_b'=\Gamma^{-1}(H_b)$, we fit the mesh of $H_a$ onto the geometry of $H_b'$. To accomplish the fitting, an optimization framework similar to [26] is employed. Each vertex $v_i$ in the mesh surface of $H_a$ is influenced by a transition vector $T_i$. We wish to find a set of transition vectors that move all vertices on $H_a$ to a deformed surface $H_a'$, such that $H_a'$ matches well with $H_b'$.

The first objective of a good match is that $H_a'$ should be as close as possible to the target shape $H_b'$. For this purpose, our objective function holds a term measuring the sum of squared distances between each vertex on $H_a$ and the reference surface $H_b'$. Simply moving each vertex on $H_a$ to its closest point on $H_b'$ may not result in an attractive mesh since neighboring parts of $H_a$ could be mapped to disparate parts of $H_b'$, and vice-versa. A smoothness term is necessary during the optimization to avoid this disparity. Our smoothness term tries to minimize the difference between the transition vectors on neighboring vertices. In summary, the objective function is defined as:

$$E_f=\sum_{i=1}^{m}\left\|T_i-T_i^0\right\|^2+\sum_{\{i,j|(v_i,v_j)\in edges(H_a)\}}\left\|T_i-T_j\right\|^2 \tag{11}$$

where $T_i^0$ is the transition vector moving the vertex $v_i$ to the closest compatible point on $H_b'$ and $m$ is the number of vertices on $H_a$. As mentioned in [26], a point on $H_a$ and a point on $H_b'$ is compatible if the surface normals at each point are no more than $90^\circ$ apart so that the front-facing surfaces will not be matched to the back-facing surfaces. The $T_i$ s that minimize $E_f$ should satisfy

$$\frac{\partial E_f}{\partial T_i}=T_i-T_i^0+\sum_{v_j\in\Pi(v_i)}(T_i-T_j)=0, \tag{12}$$

which leads to a linear equation system

$$(n+1)T_i-\sum_{v_j\in\Pi(v_i)}T_j=T_i^0 \tag{13}$$

where $\Pi(v_i)$ contains the one-ring neighborhood vertices of $v_i$, and $n$ is the number of vertices in $\Pi(v_i)$. Equation (13) satisfies the convergence condition of Gaussian-Seidal method for linear equation system [48], so the optimized $T_i$ s could be determined iteratively through the update

$$T_i=\frac{1}{n+1}(T_i^0+\sum_{v_j\in\Pi(v_i)}T_j). \tag{14}$$

Since Eq.(11) is in a quadratic form, the optimum determined by this update is global.

An iteration algorithm is conducted to match vertices of $H_a$ onto the target surface $H_b'$:

1) The iteration starts by moving every vertex $v_i\in H_a$ to the position $\tilde{\mathrm{E}}(v_i)$;
2) The $T_i^0$ of every vertex $v_i$ is evaluated;
3) Determine $T_i$ s for $v_i$ s which minimizes $E_f$ by the iterative update scheme defined in Eq.(14);
4) Move vertex $v_i$ to a new position $v_i+T_i$;
5) Evaluate $T_i^0$ s of all $v_i$ s, if any $\|T_i^0\|>\varepsilon$ (where $\varepsilon$ is a terminal threshold, e.g., $\varepsilon=10^{-5}$), go back to step 3;
6) Move vertex $v_i$ to its closest position $v_i+T_i^0$ on $H_b'$.

In this algorithm, the most time-consuming step is the evaluation of $T_i^0$ s. A voxel-based method is employed to speed up this evaluation. We subdivide the bounding space of $H_b'$:

$$[x_{\min},x_{\max}]\times[y_{\min},y_{\max}]\times[z_{\min},z_{\max}]$$

into $L\times M\times N$ sub-regions with uniform width $\Delta$, where each sub-region $\Re(i,j,k)\subset\Re^3$ is defined as

$$\begin{aligned}\Re(i,j,k)=\{(x,y,z)\in\Re^3 \mid\ & x\in[x_{\min}+i\Delta,x_{\min}+(i+1)\Delta),\\ & y\in[y_{\min}+j\Delta,y_{\min}+(j+1)\Delta),\\ & z\in[z_{\min}+k\Delta,z_{\min}+(k+1)\Delta)\}\end{aligned} \tag{15}$$

A polygonal face $f\in H_b'$ is considered as contributing to a

sub-region $\Re(i, j, k)$ if its bounding box $B(f)$ satisfies

$$\Re(i, j, k) \cap B(f) \neq \phi$$

Pointers to contributed triangles are held by each sub-region $\Re(i, j, k)$. With this space subdivision, locating the points closest to a vertex $v \in H_a$ in $\Re(l, m, n)$ only require searching in the regions $i \in [l-\tau, l+\tau]$, $j \in [m-\tau, m+\tau]$, and $k \in [n-\tau, n+\tau]$. We start searching from $\tau = 1$, if there is no triangle in the indexed sub-regions, $\tau$ is increased incrementally until some triangle is found.

After surface fitting, the refined point correspondences between the shapes of $H_a$ and $H_b'$ are constructed. We then use the correspondences to formulate a detail elastic function $\mathrm{E}(\cdots)$ to establish the mapping $\Psi$ for volume parameterization.

### D. CSRBF approach for Volume Parameterization

The refined elastic function $\mathrm{E}(\cdots)$ could be defined in a mathematical manner so that every vertex $v_i \in H_a$ is mapped to a new position $v_i' \in H_a'$. This is similar to the anchor point interpolations for computing the coarse-level elastic function. Thus, RBFs is also used to determine the $\mathrm{E}(\cdots)$. However, as the number of interpolates is significantly increased here (usually in the level of thousands or even tens of thousand), using a global RBFs, will require solving a very huge linear equation system which is computationally expensive. Although the fast multipole method (e.g., [52]) can reduce the quadratic solution time into neatly linear, the compactly supported radial-basis functions (CSRBFs) discussed below is easy to use. CSRBFs with relatively small effective distance $\lambda$ will make the linear equation system very sparse. It can thus be solved with linear time complexity. The refined elastic function is formulated as

$$\mathrm{E}(v) = \alpha_0 + Av + \sum_{i=0}^{m} \beta_i \varpi(\|v - v_i\|), \tag{16}$$

where $\varpi(r) = (1-\frac{r}{\lambda})^6 (\frac{35}{3}(\frac{r}{\lambda})^2 + 6\frac{r}{\lambda} + 1)$ for $r < \lambda$, or $\varpi(r) = 0$ for $r \geq \lambda$. This CSRBF is originally introduced by Buhmann in [53] and has been proved to give a nonsingular solution of interpolation problem. By setting

$$\mathrm{E}(v_i) = v_i', \tag{17}$$

together with the compatibility conditions, the detail elastic function $\mathrm{E}(v)$ could be determine by the *biconjugate gradient method* (ref. [48]). In order to solve the linear equation system efficiently, the authors in [44] sorted the vertices according to the distances between them. However, in our tests, the elastic function $\mathrm{E}(\cdots)$ could be determined at almost the same speed with or without sorting when using the *biconjugate gradient method* proposed in [48]. By this $\mathrm{E}(\cdots)$ and the previously obtained $\Gamma(\cdots)$, the mapping $\Psi$ for volume parameterization is explicitly defined as Eq.(1).

### E. p-FFD for Volume Parameterization

Another alternative way to calculate $\mathrm{E}(\cdots)$ is through an implicit method – the p-FFD introduced in [7]. Every polygon $f_i \in H_a$ has a local coordinate frame constructed at its center $c_{f_i}$. For a vertex $\mu_i$ on the product M around $H_a$, the shortest distance, $l_{\min}$, from $\mu_i$ to all $c_{f_i}$ s is first computed. Then, all polygons on $H_a$ with the distance from its center to $\mu_i$ less than $\frac{3}{2} l_{\min}$ are located and stored in a collection P. The local coordinates $(u_p, v_p, w_p)$ of $\mu_i$ relative to the $p$th polygon $f_p$ in P is computed and stored together with a weight $\varsigma_p$. The weight $\varsigma_p$ measures the 'strength' of the local frame on $f_p$ relative to other polygons in P, and is defined as

$$\varsigma_p = \frac{1}{10^{-8} + (u_p^2 + v_p^2 + w_p^2)^{1.5}}. \tag{18}$$

Every polygon $f_p \in H_a$ has a corresponding face $f_p' \in H_a'$. Using the local frame on $f_p'$ s and $(u_p, v_p, w_p)$ of $\mu_i$, the new position $\mu_i^p$ of $\mu_i$ around $H_a'$ can be determined. In general, the $\mu_i^p$ s are not consistent. Thus, the final mapping point $\mu_i'$ of $\mu_i$ around $H_a'$ is calculated through a weighted blending with the weight $\varsigma_p$ s (ref. [6, 7]). The correspondences of $\mu_i$ s and $\mu_i'$ s actually give an implicit discrete $\mathrm{E}(\cdots)$. Comparing to the above CSRBF based approach, this implicit discrete elastic function could be computed faster. However, this function is case dependent. Using different products around the same reference model, different correspondences (i.e., different implicit elastic functions) have to be recomputed.

## V. RESULTS AND APPLICATIONS

Our first example is the design automation of apparel product – also called *made-to-measure*. As shown in Fig. 3, the dress M is originally designed on the reference human body $H_a$ that is scanned and reconstructed from a fashion-model A. If a client B wants to buy this dress which does not fit for her body, the dress has to be customized for the body of B. First, the human body $H_b$ for B is scanned and reconstructed using the approach in [54]. The volume parameterization technique is then applied to construct a new dress $\mathrm{M}_{\mathrm{new}}$ for the client B. Finally, the 3D model of $\mathrm{M}_{\mathrm{new}}$ is cut into pieces and flattened into 2D patterns (using the approach of [18] or [19]) which will be used for fabricating the dress. In this example, the anchor points are automatically extracted by a feature-based approach [55]. Of course, they can also be interactively specified.

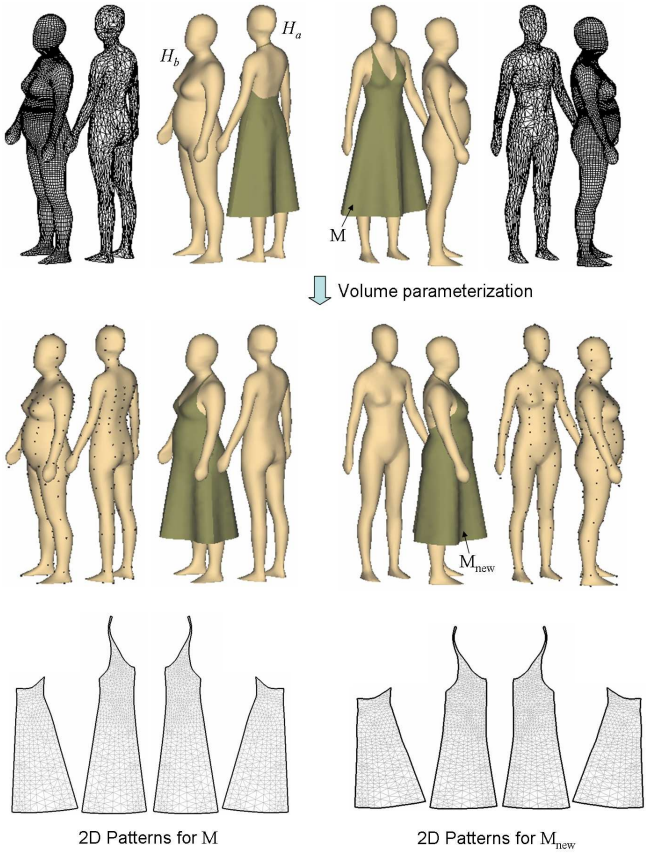


Fig. 3. Using the volume parameterization technique to automatically design a customized dress for the human body $H_b$., where the dress M is originally designed on the body of $H_a$; the connectivities on $H_a$ and $H_b$ are inconsistent (the top row); after applying the mapping of volume parameterization on M, a customized product $M_{new}$ for $H_b$ has been reconstructed (the middle row); the bottom row gives the 2D patterns for M and $M_{new}$, which can be applied in manufacturing; the black nodes on the human body (the middle row) are anchor points.

In the mapping $\Psi(t)$ of volume parameterization defined in Eq.(1), we inverse the order of applying $\mathrm{E}(\cdots)$ and $\Gamma(\cdots)$ as described in [35], where the rigid body transformation is first applied and then followed by an elastic warping as

$$\Psi'(t) = ((1-t)\mathrm{I} + t\mathrm{E})(R(t\theta_x, t\theta_y, t\theta_z)\Omega_a + tT). \quad (19)$$

In our investigation, we find that the rotation is not linear for the warping function defined in Eq.(19) (i.e., the order in [35]). This is because the elastic term $\mathrm{E}(\cdots)$ is determined relative to $R(t\theta_x, t\theta_y, t\theta_z)\Omega_a$ but not $\Omega_a$ so that the $\mathrm{E}(\cdots)$ is also sensitive to the Euler angles, $\theta_x, \theta_y, \theta_z$. When $t$ is changed, the rotation in $\Psi'(t)$ is changed proportionally to $R(t\theta_x, t\theta_y, t\theta_z)$ multiplied by the rotation in $t\mathrm{E}(\cdots)$ (i.e., nonlinearly). In our method (the $\Psi(t)$ defined in Eq.(1)), the $\mathrm{E}(\cdots)$ is insensitive to the Euler angles such that the rotation is changed linearly in $\Psi(t)$ with $t$. This effect is shown in the example of Fig. 4 where the rotation is changed linearly with $\Psi(t)$, but nonlinearly with $\Psi'(t)$.

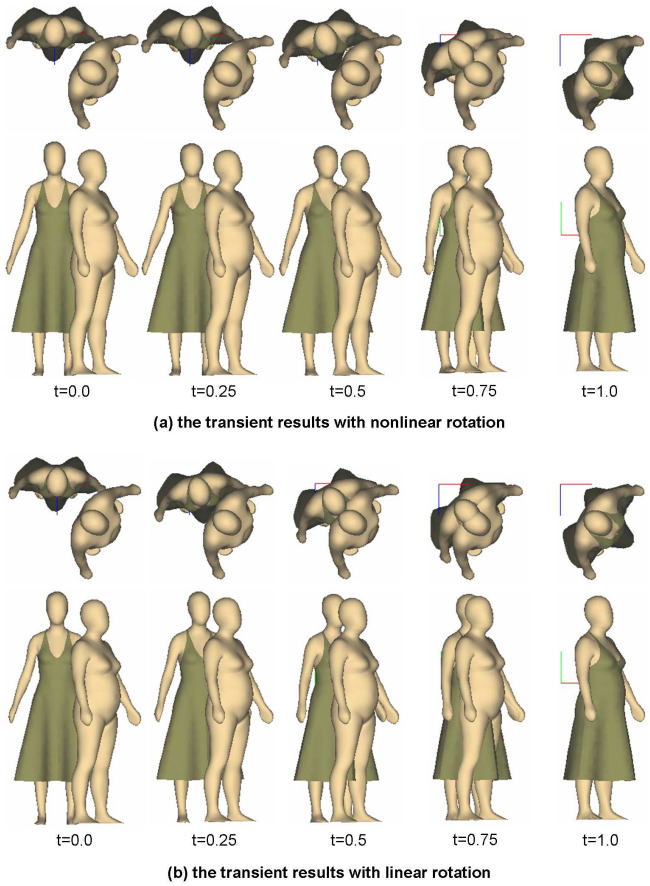


Fig. 4. The investigation about the order of applying the rigid transformation and the elastic warping. For the order of rigid transformation followed by elastic warp, the rotation is nonlinear (a), while the rotation is linear by our mapping defined in Eq.(1) (result in (b)).

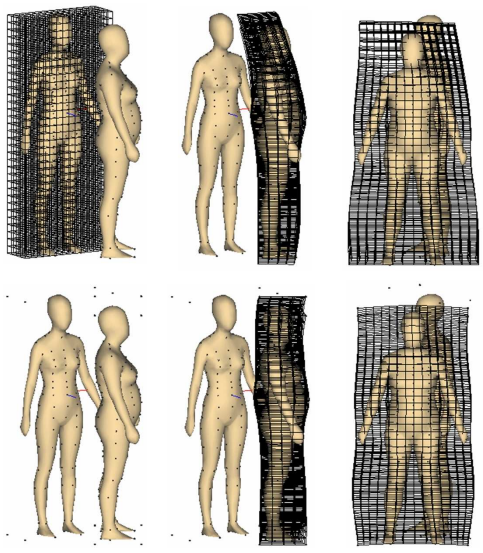

Fig. 5. Anchor points can be added in the space around reference models; the example space warping without (top) vs. with (bottom) corner anchor points are compared.

The anchor points in our volume parameterization are not necessary to be on the surface of the reference models, more anchor points could also be added in $\Omega_a$ and $\Omega_b$ to achieve

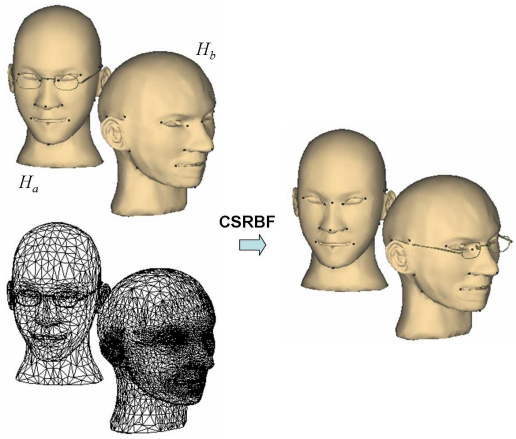


Fig. 8. Example III: an application for design automation of glasses on two head models with different connectivities.

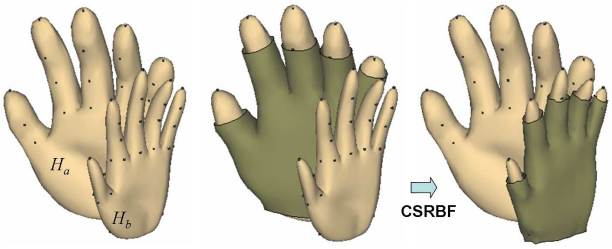


Fig. 9. Example IV: an example of hand and glove; the two reference models are with anchor points defined interactively (top right) and with inconsistent mesh connectivity (top left); after designing a glove on $H_a$ (bottom left), the glove is automatically constructed on $H_b$ (bottom right) by our volume parameterization.

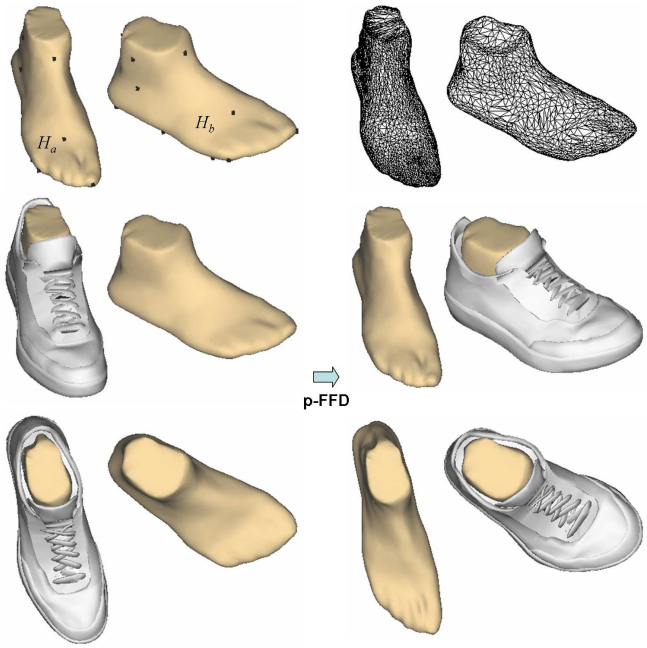


Fig. 10. Example V: an example in shoe industry.

finer control of space warping. See in Fig. 5, eight anchor points at the corner of the bounding box of $H_a$ and $H_b$ are added to achieve a better control of space warping.

In the following, we compare the results from the CSRBF-based volume parameterization and the p-FFD based parameterization. In CSRBFs, an effective distance $\lambda$ needs to be specified. For any vertex on the product M around $H_a$, if its distance to the vertices on $H_a$ is not less than $\lambda$, no radial-basis function $\varpi(\|v-v_i\|)$ will affect its position in $E(\cdots)$; i.e., its position is deformed in $E(\cdots)$ only by $A$ and $\alpha_0$. Benefited from this property, the dress reconstructed by the CSRBF-based volume parameterization on $H_b$ maintains a straight profile around the thighs (see Fig. 6(a)). However, considering the reconstructed dress by the p-FFD based parameterization, since it tries to maintain the distance of every vertex to the reference model, the parts near thighs show some unwanted distortion although they are *far* from the thighs. This difference will not be shown if the distance from every vertex on the product M to the vertices of $H_a$ is less than $\lambda$. This is because the vertices are tightly tied on the surface of $H_a$ by the radial-basis function $\varpi(\|v-v_i\|)$ s (see Fig. 6(b)). The computational statistic is shown in Table 1, from which it is not difficult to find that the CSRBF approach is a little bit slower (because of the time required for solving a huge linear equation system). In our tests, the value of $\lambda$ is chosen to be proportional to the diagonal distance of $H_a$'s bounding box.

In the apparel industry, the patterns for clothes are usually designed on a standard size (e.g., size 36 for female); then, the patterns are graded into other sizes. In current CAD systems for the garment industry, the grading is performed in 2D via offsetting related operations, which cannot guarantee the fitness. The volume parameterization technique developed in this paper provides a powerful tool for 3D grading on mannequins which ensures fitness. As shown in Fig. 7, the set of clothes in example II is graded spatially onto the bodies having the same height – 165cm but with hip girth increasing from 88cm to 112cm. The models are generated by the parametric design technique of mannequins in [54].

The third example shows an application of our technique on the design automation of glasses, where the new shape of a glass-frame can be automatically constructed (see Fig.8). The fourth example demonstrates the design automation of a glove on hand models (see Fig.9). Our last example gives the application of our volume parameterization technique in the shoe industry – the spaces around $H_a$ and $H_b$ are parameterized so that the new shoe around $H_b$ is automatically created following the shape of foot $H_b$ (see Fig.10), where the spatial relationship between the shoe and $H_a$ is retained while reconstructing the shoe on $H_b$.

## VI. LIMITATIONS

The current implementation of our approach shows several limitations:

- One is that our approach is a forward optimization approach, i.e., the bijective mapping between the spaces $\Omega_a$ and $\Omega_b$ is not given. Thus, the mapping $\Psi$ cannot guarantee that there is no self-intersection during shape deformation. Recently, in the computer graphics area, some volume-grid or also called shell-based approaches [56, 57]

TABLE I
COMPUTATIONAL STATISTIC

| Example | Figures | Parameterization method | Computing time | Surface fitting time | $H_a$ node no. | $H_a$ face no. | $H_b$ node no. | $H_b$ face no. | M node no. | M face no. |
|---|---|---|---|---|---|---|---|---|---|---|
| I | 3 & 6a | CSRBF ($\lambda$=10) | 17.0s | 22.0s | 2,000 | 3,936 | 11,072 | 11,040 | 1,900 | 3,643 |
| | 6a | p-FFD | 0.3s | | | | | | | |
| II | 6b | CSRBF ($\lambda$=10) | 19.0s | 7.8s | 1,960 | 3,916 | 2,232 | 4,460 | 1,986 | 3,771 |
| | 6b | p-FFD | 0.2s | | | | | | | |
| | 7 | CSRBF ($\lambda$=10) | 19.0s | 24.3s | 1,960 | 3,913 | 11,520 | 11,488 | 1,986 | 3,771 |
| III | 8 | CSRBF ($\lambda$=5) | 8.5s | 22.7s | 1,399 | 2,794 | 6,093 | 12,182 | 608 | 1,224 |
| IV | 9 | CSRBF ($\lambda$=8) | 6.1s | 8.0s | 1,982 | 3,960 | 2,169 | 4,334 | 1,457 | 2,780 |
| V | 10 | p-FFD | 1.3s | 14.3 | 7,026 | 14,044 | 1,610 | 3,216 | 2,171 | 3,636 |

[a]All tests are performed on a PC with AMD Althon XP-M 2400+ CPU (1.6GHz) + 512MB RAM.

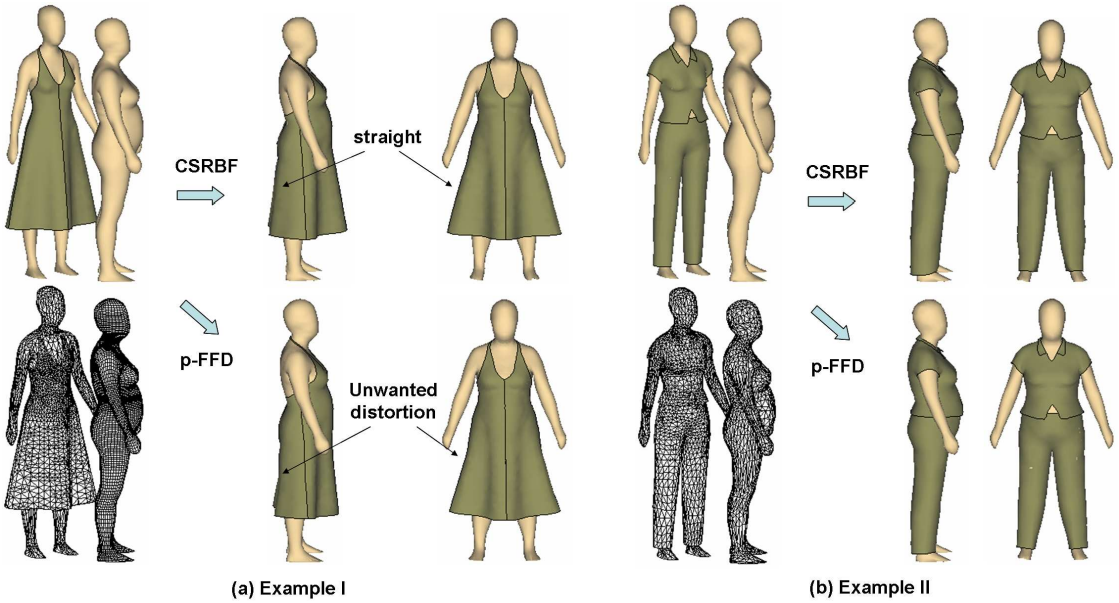


Fig. 6. Comparison of the results from the CSRBF-based volume parameterization and the p-FFD based volume parameterization.

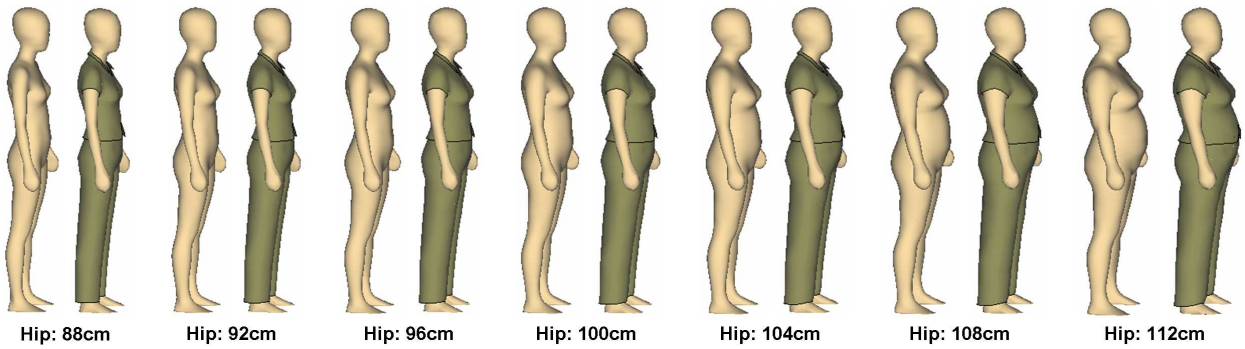


Fig. 7. On design automation of clothes on the human bodies with hip/height ratio changed (height: 165cm).

have been developed for the similar purpose of space mapping. They are in fact still mesh-based approaches. Although claiming intersection-prevented, they actually cannot really guarantee non-self-intersection if the grids intersect each other in the global sense (e.g., the space around hand intersect the space around thigh on a human body).

- Secondly, the topology consistency of our $\Psi$ will be broken if the anchor points on reference models are wrongly matched. For example in Fig.9, if an anchor point on the thumb of $H_a$ is mapped to one on the ring-finger of $H_b$, unexpected distortions will be shown in $\Psi$.
- Only points served as semantic features are considered in our approach. Although edges and patches can be thought as a collection of points, the extension of our current implement onto models with feature edges and patches is not straightforward.
- Lastly, our current approach lacks metrics to measure the quality of a mapping. All results are visually measured.

## VII. CONCLUSION

In this paper, we present a technique called volume parameterization which serves as the geometric kernel for the design automation of customized free-form products. Volume parameterization is in fact a problem about how to establish a mapping between the spaces around two reference models. With the help of this mapping, a free-form product specified around one reference model can be transferred onto other reference models. The mapping is separated into a rigid body transformation and an elastic warping. To determine the mapping, a three-stage approach is developed. In the first stage, the rigid body transformation and the coarse-level warping are computed by using anchor points which are considered as feature constraints. A surface fitting process is then applied to the coarsely warped model to construct the correspondences between reference models with inconsistent meshes. Finally, the space mapping $\Psi$ for volume parameterization is defined mathematically and algorithmically.

Based on the limitations of our approach, in the future, we would like to develop some mesh-free method to achieve a bijective mapping so that the property of non-self-intersection could be elegantly preserved during the design automation of customized free-form products. Introducing a mechanism to adaptively add anchor points is under our research plan. Considering about anchor points in the current approach – all are with the same importance, this may not reflect the practice. Therefore, developing a mapping method with weighted anchor points could be another possible further research direction.

## ACKNOWLEDGEMENTS

The authors would like to acknowledge the helpful comments given by the reviewers. This work was partially supported by the Hong Kong RGC/CERG grant CUHK/412405.

## REFERENCES

[1] M. E. Mortenson, *Geometric Modeling*, New York: Wiley, 1985.
[2] C. M. Hoffmann, *Geometric and Solid Modeling*. San Mateo, Calif.: Morgan Kaufmann, 1989.
[3] W. Bouma, X. Chen, I. Fudos, C. Hoffmann, and P. J. Vermeer, *An Electronic Primer on Geometric Constraint Solving*. Available: http://www.cs.purdue.edu/homes/cmh/electrobook/intro.html
[4] S. R. Marschner, B. Guenter, and S. Raghupathy, "Modeling and rendering for realistic facial animation", in *Proceedings of 11th Eurographics Workshop on Rendering*, 2000, pp.231-242.
[5] H. Seo, and N. Magnenat-Thalmann, "An example-based approach to human body manipulation", *Graphical Models*, vol.66, no.1, 2004, pp.1-69.
[6] K. G. Kobayashi, and K. Ootsubo, "t-FFD: free-form deformation by using triangular mesh", in *Proceedings of the Eighth ACM Symposium on Solid Modeling and Applications*, 2003, pp.226-234.
[7] C. C. L. Wang, Y. Wang, and M. M. F. Yuen, "Design automation for customized apparel products", *Computer-Aided Design*, vol.37, no.7, 2005, pp.675-691.
[8] V. Kraevoy, and A. Sheffer, "Cross-parameterization and compatible remeshing of 3D models", *ACM Trans. on Graphics*, vol.23, no.3, 2004, pp. 861-869.
[9] J. Schreiner, A. Asirvatham, E. Praun, and H. Hoppe, "Inter-surface mapping", *ACM Trans. on Graphics*, vol.23, no.3, 2004, pp.870-877.
[10] M. S. Floater, and K. Hormann, "Recent advances in surface parameterization", In *Multiresolution in Geometric Modeling*, 2003, pp.259-284.
[11] M. S. Floater, "Parametrization and smooth approximation of surface triangulations", *Computer Aided Geometric Design*, vol.14, no.3, April 1997, pp.231-71.
[12] A. Sheffer, and E. de Sturler, "Parameterization of faceted surfaces for meshing using angle based flattening", *Engineering with Computers*, vol.17, no.3, 2001, pp.326-337.
[13] P. V. Sander, J. Snyder, S. J. Gortler, and H. Hoppe, "Texture mapping progressive meshes", in *Proceedings of SIGGRAPH 2001*, pp.409-416, 2001.
[14] A. Sheffer, and E. de Sturler, "Smoothing an overlay grid to minimize linear distortion in texture mapping", *ACM Trans. on Graphics*, vol.21, no.4, 2002, pp.874-890.
[15] B. Levy, S. Petitjean, N. Ray, and J. Maillot, "Least squares conformal maps for automatic texture atlas generation", *ACM Trans. on Graphics*, vol.21, no.3, 2002, pp.362-71.
[16] M. Desbrun, M. Meyer, and P. Alliez, "Intrinsic parameterizations of surface meshes", *Computer Graphics Forum*, vol.21, no.3, 2002, pp.209-218.
[17] S. Yoshizawa, A. Belyaev, and H. P. Seidel, "A fast and simple stretch-minimizing mesh parameterization", in *Proceedings of Shape Modeling and Applications 2004*, pp.200-208, 2004.
[18] C. C. L. Wang, S. S. F. Smith, and M. M. F. Yuen, "Surface flattening based on energy model", *Computer-Aided Design*, vol.34, no.11, 2002, pp.823-833.
[19] C. C. L. Wang, K. Tang, and B. M. L. Yeung, "Freeform surface flattening by fitting a woven mesh model", *Computer-Aided Design*, 2005, vol.37, no.8, pp.799-814.
[20] M. Alexa, "Recent advances in mesh morphing", *Computer Graphics Forum*, vol.22, no.2, 2002, pp.173-196.
[21] A. Lee, D. Dobkin, W. Sweldens, and P. Schröder, "Multiresolution mesh morphing", in *Proceedings of ACM SIGGRAPH 1999*, 1999, pp.343-350.
[22] T. Michikawa, T. Kanai, M. Fujita, and H. Chiyokura, "Multiresolution interpolation meshes", in *Proceedings of Ninth Pacific Conference on Computer Graphics and Applications*, 2001, pp.60-69.
[23] E. Praun, W. Sweldens, and P. Schröder, "Consistent mesh parameterizations", in Proceedings of SIGGRAPH 2001, pp.179-184, 2001.
[24] J. L. Lin, J. H. Chuang, C. C. Lin, and C. C. Chen, "Consistent parametrization by quinary subdivision for remeshing and mesh metamorphosis", in *Proceedings of the 1st International Conference on Computer Graphics and Interactive Techniques in Australasia and South East Asia*, 2003, pp.151-158.
[25] V. Kraevoy, A. Sheffer, and C. Gotsman, "Matchmaker: constructing constrained texture maps", *ACM Trans. on Graphics*, vol.22, no.3, 2003, pp.326-333.
[26] B. Allen, B. Curless, and Z. Popović, "The space of human body shapes: reconstruction and parameterization from range scans", *ACM Trans. on Graphics*, vol.22, no.3, 2003, pp.587-594.
[27] J.S.M. Vergeest, S. Spanjaard, and Y. Song, "Directed mean Hausdorff distance of parameterized freeform shapes in 3D: a case study", *The Visual Computer*, vol.19, no.7-8, 2003, pp.480-492.
[28] K.M. Yu , and W.M. Zhu, "Dimension-driven parameterized design of free form objects", in *Proceedings Geometric Modeling and Processing 2000 - Theory and Applications*, 2000, po.90-100.
[29] T. Sederberg, and S. Parry, "Free-form deformations of solid geometric models", *Computer Graphics*, vol.20, 1986, pp.151-160.
[30] S. Coquillart, "Extended free-form deformations: a sculpting tool for 3D geometric modeling", *Computer Graphics*, vol.24, no.4, 1990, pp.187-196.
[31] Y. K. Chang, and A. P. Rockwood, "A generalized de Casteljau approach to 3D free-form deformation", *Computer Graphics*, vol.28, no.4, 1994, pp.257-260.
[32] W. Hsu, J. Hughes, and H. Kaufmann, "Direct manipulations of free-form deformations", *Computer Graphics*, vol.26, no.2, 1992, pp.177-184.
[33] R. MacCracken, and K. Joy, "Free-form deformations with lattices of arbitrary topology", *Computer Graphics*, 1996, pp.181-189.
[34] J. Hua, and H. Qin, "Scalar-field-guided adaptive shape deformation and animation", *The Visual Computer*, vol. 20, no.1, 2004, pp.47-66.

[35] D. Cohen-Or, A. Solomovic, and D. Levin, "Three-dimensional distance field metamorphosis", *ACM Trans. on Graphics*, vol.17, no.2, 1998, pp. 116-141.
[36] M. Alexa, and M. Muller, "Representing animations by principal components", *Computer Graphics Forum*, vol.19, no.3, pp.411-418.
[37] A. Shamir, and V. Pascucci, "Temporal and spatial level of details for dynamic meshes", in *Proceedings of the ACM symposium on Virtual reality software and technology*, 2001, pp.77-84.
[38] V. V. Savchenko, A. A. Pasko, O. G. Okunev and T. L. Kunii, "Function representation of solids reconstructed from scattered surface points and contours", *Computer Graphics Forum*, vol.14, no.4, 1995, pp.181-188.
[39] J. C. Carr, R. K. Beatson, J. B. Cherrie, T. J. Mitchell, W. R. Fright, B. C. McCallum and T. R. Evans, "Reconstruction and representation of 3D objects with radial basis functions", in Proceedings of SIGGRAPH '01, pp. 67–76, 2001.
[40] Y. Ohtake, A. Belyaev, and H.-P. Seidel, "A multi-scale approach to 3D scattered data interpolation with compactly supported basis functions", in *Proceedings of Shape Modeling International*, 2003, pp.153-164.
[41] Y. Ohtake, A. Belyaev, M. Alexa, G. Turk, H.-P. Seidel, "Multi-level partition of unity implicits", *ACM Trans. on Graphics*, vol.22, no.3, 2003, pp.463-470.
[42] G. Turk, and J.F. O'Brein, "Modelling with implicit surfaces that interpolates", *ACM Transactions on Graphics*, vol.21, no.4, 2002.
[43] E. Carmel, D. Cohen-Or, "Warp-guided object-space morphing", *The Visual Computer*, vol.13, no.9-10, 1997, pp.465-478.
[44] N. Kozhekin, V. Savchenko, M. Senin, and I. Hagiwara, "An approach to surface retouching and mesh smoothing", *The Visual Computer*, vol.19, no.7-8, 2003, pp. 549-564.
[45] C. Rose, M. Cohen, and B. Bodenheimer, "Verbs and adverbs: multidimensional motion interpolation using RBF", *IEEE Computer Graphics and Applications*, vol.18, no.5, 1998, pp.32–40.
[46] J. P. Lewis, M. Cordner, N. Fong, "Pose space deformations: a unified approach to shape interpolation and skeleton-driven deformation", in *Proceedings of SIGGRAPH '00*, pp. 165–172, 2000.
[47] K. S. Arun, T. S. Huang, and S. D. Blostein, "Least-squares fitting of two 3-D point sets", *IEEE Transs on Pattern Analysis and Machine Intelligence*, vol.9, no.5, 1987, pp.698-700.
[48] W. H. Press, B. P. Flannery, S. A. Teukolsky, W. T. Vetterling, *Numerical Recipes in C : the Art of Scientific Computing* (2nd ed.), Cambridge: Cambridge University Press, 1995.
[49] K. Shoemake, "Animating rotation with quaternion curves", in *Proceedings of the 12th Annual Conference on Computer Graphics and Interactive Techniques*, 1985, pp.245-254.
[50] N. Dyn, "Interpolation and approximation by radial and related functions", in *Approximation Theory VI*, L. L. Schumaker, C. K. Chui, and J. D. Ward, eds., 1987, pp.211-234.
[51] R. Bellman, *Introduction to Matrix Analysis*, McGraw-Hill, 1960.
[52] R. Beatson, and L. Greengard, "A short course on fast multipole methods", in *Wavelets, Multilevel Methods and Elliptic PDEs*, M. Ainsworth, J. Levesley, W. Light and M. Marletta (eds.), 1997, pp.1-37, Oxford University Press.
[53] M. D. Buhmann, "A new class of radial basis functions with compact support", *Mathematics of Computation*, vol.70, 2000, pp.307-318.
[54] C. C. L. Wang, "Parameterization and parametric design of mannequins", *Computer-Aided Design*, vol.37, no.1, 2005, pp.83-98.
[55] C. C. L. Wang, T. K. K. Chang, and M. M. F. Yuen, "From laser-scanned data to feature human model: a system based on fuzzy logic concept", *Computer-Aided Design*, vol.35, no.3, 2003, pp.241-253.
[56] J. Peng, D. Kristjansson, and D. Zorin, "Interactive modeling of topologically complex geometric detail", *ACM Transactions on Graphics*, vol.23, no.3, 2004, pp.635-643.
[57] S.D. Porumbescu, B. Budge, L. Feng, and K.I. Joy, "Shell maps", *ACM Transactions on Graphics*, vol.24, no.3, 2005, pp.626-633.